k·p theory of the Franz-Keldysh effect

Jörg Hader,* Norbert Linder, and Gottfried H. Döhler
Institut für Technische Physik I, Universität Erlangen, Erwin-Rommel-Strasse 1, D-91058 Erlangen, Germany
(Received 13 September 1996)

We use the **k·p** formalism to calculate Franz-Keldysh (FK) absorption spectra in direct-band-gap III-V semiconductors. This method allows us to include band anisotropy and nonparabolicity as well as band mixing. With **k·p** models of various complexity, we investigate how these phenomena influence the main features of the electroabsorption using GaAs as an example. We show that the dependence of the FK absorption on the polarization of the incoming light can be understood in analogy to quasi-two-dimensional systems by mostly decoupled heavy- and light-hole bands involving the anisotropy of the bulk-momentum matrix elements. On the other hand, the FK absorption tail and the periods of the FK oscillations are mainly determined by the realistic energy dispersions of the bands. We discuss the applicability and the limits of simplified models and demonstrate that for most cases the field-induced interband mixing is negligible in comparison with the zero-field coupling of the bands. As an application, we show the consequences for the widely used method to determine the electric field from the FK oscillation periods measured by absorption or photoreflectance experiments. Most of the basic features have been observed in experiments. The qualitative details are of general validity. [S0163-1829(97)00707-8]

I. INTRODUCTION

The influence of a homogeneous electric field **F** on the optical properties of a semiconductor is one of the basic problems of optoelectronics. Although the potential-energy term $e\mathbf{F}\cdot\mathbf{x}$ has a very simple form, attempts to develop a realistic picture of the situation including all aspects of crystal physics have to use certain approximations and progress was only gradually achieved.

In 1958, Franz[1] and Keldysh[2] used the isotropic effective-mass approximation (EMA) to show that the influence of an electric field leads to an exponential tail of the absorption coefficient of a direct semiconductor for photon energies $\hbar\omega$ smaller than the gap energy E_g. The reason is that the Bloch states of the unperturbed crystal become coupled along the direction of the field. The resulting states decay exponentially into the gap region and oscillate within the bands (Fig. 1). Therefore, the absorption coefficient $\alpha(\omega)$, which is proportional to the square of the overlap between the electron and hole states, exhibits the above-mentioned exponential tail for $\hbar\omega<E_g$ and the well-known Franz-Keldysh (FK) oscillations around the zero-field spectrum due to interference of the oscillating parts of the states for $\hbar\omega>E_g$. The exponential tail, as well as the periods and amplitudes of the FK oscillations, increases with F.

In the late 1960s Aspnes[3,4] greatly improved the understanding of the FK effect. He expanded the work of Tharmalingam[5] and Penchina,[6] who had calculated the electroabsorption in direct and indirect semiconductors, respectively, in terms of Airy functions, assuming an isotropic medium. The Airy functions are the solutions for electrons and holes in the presence of a uniform electric field in the EMA envelope-function formalism. Aspnes obtained closed-form expressions for the FK absorption in the vicinity of all kinds of critical points of the combined density of states M_i ($i=0,1,2,3$), for anisotropic effective masses and arbitrarily oriented fields.

In order to get quantitatively correct spectra the Coulomb interaction cannot be neglected. This was pointed out by Dow and Redfield[7] and Blossey.[8] They gave exact numerical solutions of the problem based on the EMA with isotropic effective masses. A semiempirical approach that is able to account partially for the carrier-lattice interaction, band anisotropy, lifetime broadening and surface effects in addition to the Coulomb interaction was proposed by Rees.[9] Using an expression that mainly consists of a convolution of the zero-field absorption (including those effects) and a broadening due to the field-induced changes expressed in terms of Airy functions, he achieved satisfactory agreement with experimental results. Comparisons with experimental data were also given by Galbraith and Ryvkin,[10] who further refined

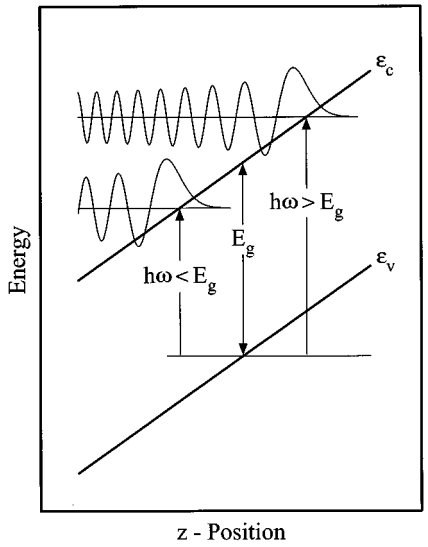

FIG. 1. Schematic drawing of conduction- and valence-band edges, the envelopes of typical FK eigenstates, and possible optical transitions of a semiconductor in a homogeneous electric field.

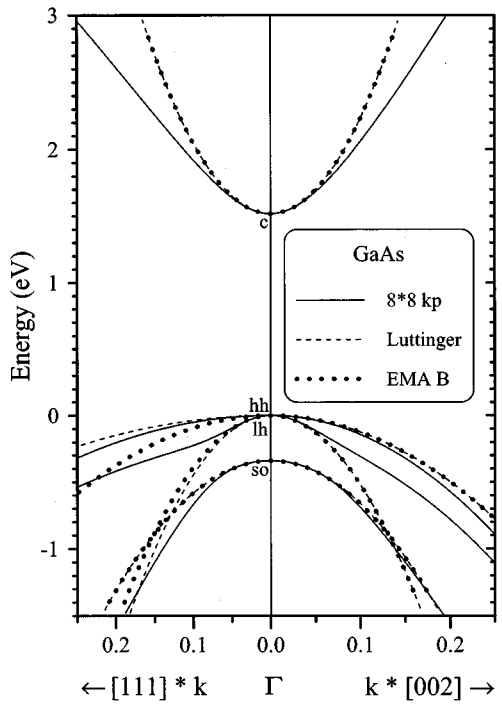

FIG. 2. Conduction- and valence-band dispersions of GaAs, calculated within the 8×8 **k·p** model, the Luttinger model, and the EMA *B*.

Rees's model, and by Linder *et al.*,[11] who focused their attention on the importance of excitonic effects with regard to a quantitative description of the effect.

In order to obtain closed-form expressions for the FK absorption at photon energies above as well as below E_g, all approaches so far used the EMA, i.e., they assumed decoupled parabolic bands. In most direct semiconductors this is only a crude approximation to the actual band structure. In such materials the light- and heavy-hole bands are degenerate at the valence-band maximum and the interaction between states of different bands causes distinct nonparabolicities, especially in the lowest conduction and the light-hole band, and strong warping of the heavy-hole band (cf. Fig. 2).

Initial efforts to take into account the complex structure of the fourfold degenerate valence bands in diamond and zinc-blende crystals were made by Keldysh *et al.*[12] Their results include the coupling between light- and heavy-hole bands, but are valid only for photon energies far below E_g. For this spectral region the authors give estimates about the dependence of the absorption coefficient on the orientation of the polarization vector **e** of the incoming light relative to the direction of the applied electric field.

The **k·p** Hamiltonian as introduced by Kane[13] represents the realistic coupled band structure in the vicinity of the Γ point in the absence of a perturbing potential. Using this Hamiltonian in the **k**-space representation of the FK problem (without the Coulomb interaction) leads to a system of coupled differential equations from which, as we will show, the FK eigenstates, as the basis for the determination of the absorption coefficient, can be evaluated numerically. Using **k·p** Hamiltonians of different complexity and comparing the results with those of EMA calculations allows us to investigate the influences of nonparabolicity. Due to the orientation dependence of the **k·p** Hamiltonian, reflecting the nonspherical symmetry of the crystal, the polarization dependence of the absorption is implicitly taken into account.

Sheen and Pollak[14] deduced a formula from the EMA expressions for the electroabsorption that allows one to determine either the electric field (if the reduced effective mass $\mu^\star$ is known) or the reduced effective mass (if the field is given) from the positions of the extrema of the FK oscillations. The pronounced nonparabolicity of conduction and valence bands, however, makes it dubious whether it is really possible to use this relation to derive **F** or $\mu^\star$ from experimental FK spectra. Our calculations prove that a slightly modified relation still holds in spite of the deviations from the parabolic EMA dispersions in those energy regions where the oscillations occur.

Since the excitonic interaction is neglected in our calculations our spectra will not give absolute evidence about absorption strength and the absorption edge will be reproduced incorrectly. Nevertheless, the effects of band mixing are mostly insensitive to this since the additional isotropic Coulomb potential primarily changes the states close to E_g. Thus it should not essentially affect our results, which are focused on the spectral regions ''far'' (i.e., many exciton Rydberg energies away) from E_g.

In Sec. II the basic theoretical concepts of the **k·p** approach and its numerical realization will be presented. In Sec. III we will show typical FK spectra obtained from our calculations and compare them to EMA and zero-field results in order to explain the changes induced by the realistic band structure. Afterward, the influences of the features included in our calculations are studied in detail, first the nonparabolicity effects and second the polarization dependence.

II. THEORY

A. Coupled-band FK eigenstates

The **k·p** method is a well-known tool to include band coupling into calculations of the band structure. It is based on an expansion of the crystal Hamiltonian in terms of Bloch functions in the vicinity of high-symmetry points of the Brillouin zone. Through the introduction of a small set of semiempirical parameters, high accuracy with respect to energies and the explicit shape of the wave functions can be achieved. Since the direct absorption in semiconductors such as GaAs involves only states close to the Γ point, this method is well suited to calculate the states for the FK absorption, taking into account all aspects of the realistic dispersion, i.e. nonparabolicity, band mixing, and effects of anisotropy. Following the lines of Kane[13] for transferring the unperturbed single-particle lattice Hamiltonian

$$H_0=\frac{p^2}{2m}+V_G(\mathbf{x})+\frac{\hbar}{4m^2c^2}[\boldsymbol{\sigma}\times\boldsymbol{\nabla}V_G(\mathbf{x})]\cdot\mathbf{p} \qquad (1)$$

from the real-space representation to the **k·p** representation $H^{\mathbf{k}\cdot\mathbf{p}}$, it is straightforward to do the same for the potential term $e\mathbf{F}\cdot\mathbf{x}$. The solutions $\boldsymbol{\Psi}^{F,\varepsilon}(\mathbf{x})$ of Schrödinger's equation

$$(H_0+e\mathbf{F}\cdot\mathbf{x}-\varepsilon)\boldsymbol{\Psi}^{F,\varepsilon}(\mathbf{x})=0 \qquad (2)$$

TABLE I. Lattice-symmetric functions $u_{n\mathbf{0}}$, which are the basis states of the irreducible representations Γ_6, Γ_7, and Γ_8 of the Γ-point double group in the zinc-blende structure. They have the symmetry of angular momentum eigenstates $|j,m(j_1,j_2)\rangle$. The conduction-band (CB) states posesss Γ_6, heavy- (hh) and light-hole (lh) Γ_8, and split-off (SO) hole Γ_7 symmetry. The notation follows that of Dresselhaus (Ref. 33).

Representation	Bands	Angular momentum eigenstates	
Γ_6	CB	$\|1/2,+1/2(0,1/2)\rangle$	$\|s\rangle\uparrow$
		$\|1/2,-1/2(0,1/2)\rangle$	$\|s\rangle\downarrow$
Γ_7	SO	$\|1/2,+1/2(1,1/2)\rangle$	$1/\sqrt{3}[-\|x\rangle-i\|y\rangle]\downarrow-\|z\rangle\uparrow$
		$\|1/2,-1/2(1,1/2)\rangle$	$1/\sqrt{3}[-\|x\rangle+i\|y\rangle]\uparrow+\|z\rangle\downarrow$
Γ_8	hh	$\|3/2,+3/2(1,1/2)\rangle$	$1/\sqrt{2}[\|x\rangle+i\|y\rangle]\uparrow$
		$\|3/2,-3/2(1,1/2)\rangle$	$1/\sqrt{2}[\|x\rangle-i\|y\rangle]\downarrow$
	lh	$\|3/2,+1/2(1,1/2)\rangle$	$1/\sqrt{6}[\|x\rangle+i\|y\rangle]\downarrow-2\|z\rangle\uparrow$
		$\|3/2,-1/2(1,1/2)\rangle$	$1/\sqrt{6}[\|x\rangle-i\|y\rangle]\uparrow+2\|z\rangle\downarrow$

are expanded in terms of the Γ-point Bloch functions $u_{n\mathbf{0}}(\mathbf{x})$

$$\Psi^{F,\varepsilon}(\mathbf{x})=\sum_{n,\mathbf{k}} c_n^{F,\varepsilon}(\mathbf{k})\underbrace{u_{n\mathbf{0}}(\mathbf{x})e^{i\mathbf{k}\cdot\mathbf{x}}}_{\chi_{n\mathbf{k}}(\mathbf{x})}. \tag{3}$$

By multiplication with $\chi^{\star}_{n'\mathbf{k}'}$ from the left-hand side and integration over the crystal volume, using

$$\langle\chi_{n'\mathbf{k}'}|e\mathbf{F}\cdot\mathbf{x}|\chi_{n\mathbf{k}}\rangle=ie\mathbf{F}\delta_{nn'}\delta(\mathbf{k}-\mathbf{k}')\nabla_{\mathbf{k}}, \tag{4}$$

Eq. (2) transforms to a matrix equation for the $k_\parallel$ dependence of the complex coefficient functions $c^{F,\varepsilon}_{n,\mathbf{k}_\perp}(k_\parallel)$:

$$\sum_n\left[H^{\mathbf{k}\cdot\mathbf{p}}_{n'n}(k_\parallel,\mathbf{k}_\perp)+\delta_{n'n}ieF\frac{\partial}{\partial k_\parallel}\right]c^{F,\varepsilon}_{n,\mathbf{k}_\perp}(k_\parallel)=\delta_{n'n}\varepsilon c^{F,\varepsilon}_{n,\mathbf{k}_\perp}(k_\parallel). \tag{5}$$

Here the continuous variable $\mathbf{k}$ has been separated into the components parallel ($k_\parallel$) and perpendicular ($\mathbf{k}_\perp$) to the electric field. The eigenenergy ε is treated as continuous. The discrete nature of ε due to the Wannier-Stark effect can be neglected since the Stark steps are very small and thus totally obscured by the natural lifetime line broadening present in bulk semiconductors. The FK eigenstates are multicomponent functions, the nth component of which can finally be written

$$[\Psi^{F,\varepsilon}_{\mathbf{k}_\perp}(\mathbf{x})]_n=u_{n\mathbf{0}}(\mathbf{x})\cdot e^{i\mathbf{k}_\perp\cdot\mathbf{x}_\perp}\frac{\Omega^{1/3}}{2\pi}\int dk_\parallel e^{ik_\parallel x}c^{F,\varepsilon}_{n,\mathbf{k}_\perp}(k_\parallel). \tag{6}$$

where Ω is the volume of the Wigner-Seitz cell.

The functions $u_{n\mathbf{0}}$ are specified in Table I. They have the symmetry of angular momentum eigenstates with the quantum numbers given there and transform under the operations of the double group according to states of the representations Γ_6, Γ_7, and Γ_8. Due to the first property, the spin-orbit coupling becomes diagonal in the band index n; the second helps to reduce the numerical effort. In terms of these states the $\mathbf{k}\cdot\mathbf{p}$ Hamilton matrix including the light-hole, the heavy-hole, the split-off-hole and the lowest s-like conduction bands, each being doubly Kramers degenerate, has the form given in Table II (in the matrix expansion we follow Ref. 13 and use the parameter values given in Table III). This fully coupled 8×8 matrix is the most complex one for which we calculated absorption spectra. To obtain correct band dispersions and effective masses, which the FK effect is sensitive to, the remote bands have been included via the Löwdin renormalization.[16,13,15] If these bands were taken into account explicitly one would obtain rapidly oscillating coefficient functions $c_n(k_\parallel)$ for them, which would multiply the numerical effort. A comparison of the $\varepsilon(\mathbf{k})$ dispersions in various models shows that using $\mathbf{k}\cdot\mathbf{p}$ Hamiltonians larger than 8×8 would not lead to substantial improvements in the relevant k range either.

For a matrix $H^{\mathbf{k}\cdot\mathbf{p}}$ as given by Table II, Eq. (5) can be solved only numerically. For this purpose Eq. (5) is rewritten as an integral equation

$$\mathbf{c}^{F,\varepsilon}_{\mathbf{k}_\perp}(k_\parallel)=\mathbf{c}^{F,\varepsilon}_{\mathbf{k}_\perp}(k_{\parallel0})+\int_{k_{\parallel0}}^{k_\parallel}dk'_\parallel\left[\frac{i}{eF}(H^{(\mathbf{k}_\perp,k'_\parallel)\cdot\mathbf{p}}-\varepsilon)\mathbf{c}^{F,\varepsilon}_{\mathbf{k}_\perp}(k'_\parallel)\right]. \tag{7}$$

Equation (7) has to be solved for every possible value of $\mathbf{k}_\perp$, each resulting in one vector $\mathbf{c}$ of coefficient-functions. If N is the dimension of the $\mathbf{k}\cdot\mathbf{p}$ matrix, there are N linearly independent initial conditions $\mathbf{c}^{(m)}_{\mathbf{k}_\perp}(k_{\parallel0})$, leading to N solutions $\mathbf{c}^{(m)}_{\mathbf{k}_\perp}(k_\parallel)$ ($m=0,\ldots,N-1$). Without any restriction we choose for the initial conditions

$$(c_n)^{(m)}_{\mathbf{k}_\perp}(k_{\parallel0}=0)=\frac{1}{\sqrt{\Delta_\parallel}}\delta_{mn}, \tag{8}$$

with $\Delta_\parallel$ being the length of the integration interval. In principle, the integration has to be performed over the whole first Brillouin zone. However, since increasing values of $\mathbf{k}$ correspond to states of increasing energy their contribution becomes less important for transitions with $\hbar\omega\approx E_g$. Thus the highest values we include in the calculations are $|k_\parallel|=0.7\pi/a_0$ ($0.35\pi/a_0$) and $|\mathbf{k}_\perp|=0.25\pi/a_0$ ($0.15\pi/a_0$) for GaAs (InSb). A comparison of the dispersions of the 8×8 model with that of a 16×16 $\mathbf{k}\cdot\mathbf{p}$ Hamiltonian (not shown here) indicates that the $\mathbf{k}\cdot\mathbf{p}$ models we used are still fairly correct for such values of k. Also the results of the FK calculations do not change if we extend the integration range beyond the limits as given above.

TABLE II. Fully coupled 8×8 $\mathbf{k}\cdot\mathbf{p}$ Hamilton matrix for a diamond lattice (in a.u.). The values for the constants are given in Table III and follow the notation of Cardona *et al.* (Ref. 15). $k_\pm = k_x \pm i k_y$. The matrix is Hermitian.

Γ_7^v		Γ_8^v				Γ_6^c	
$\lvert\frac{1}{2},+\frac{1}{2}\rangle$	$\lvert\frac{1}{2},-\frac{1}{2}\rangle$	$\lvert\frac{3}{2},+\frac{3}{2}\rangle$	$\lvert\frac{3}{2},+\frac{1}{2}\rangle$	$\lvert\frac{3}{2},-\frac{1}{2}\rangle$	$\lvert\frac{3}{2},-\frac{3}{2}\rangle$	$\lvert\frac{1}{2},+\frac{1}{2}\rangle$	$\lvert\frac{1}{2},-\frac{1}{2}\rangle$
$\varepsilon_{v0}-\Delta_0$ $-\frac{1}{2}\gamma_1' k^2$	0	$\frac{\sqrt{3}}{\sqrt{2}}\gamma_3' k_z k_+$	$\frac{1}{\sqrt{2}}\gamma_2'(k_x^2+k_y^2-2k_z^2)$	$\frac{\sqrt{3}}{\sqrt{2}}\gamma_3' k_z k_-$	$\frac{\sqrt{3}}{\sqrt{2}}\gamma_2'(k_x^2-k_y^2)-i\sqrt{6}\gamma_3' k_x k_y$	$i\frac{1}{\sqrt{3}}Pk_z$	$i\frac{1}{\sqrt{3}}Pk_-$
	$\varepsilon_{v0}-\Delta_0-\frac{1}{2}\gamma_s' k^2$	$\frac{\sqrt{3}}{\sqrt{2}}\gamma_2'(k_x^2-k_y^2)+i\sqrt{6}\gamma_3' k_x k_y$	$-\frac{3}{\sqrt{2}}\gamma_3' k_z k_+$	$\frac{1}{\sqrt{2}}\gamma_2'(k_x^2+k_y^2-2k_z^2)$	$-\frac{\sqrt{3}}{\sqrt{2}}\gamma_3' k_z k_-$	$i\frac{1}{\sqrt{3}}Pk_+$	$-i\frac{1}{\sqrt{3}}Pk_z$
		$\varepsilon_{v0}-\frac{1}{2}\gamma_1' k^2-\frac{1}{2}\gamma_2'(k_x^2+k_y^2-2k_z^2)$	$\sqrt{3}\gamma_3' k_z k_-$	$-\frac{\sqrt{3}}{2}\gamma_2'(k_x^2-k_y^2)+i\sqrt{3}\gamma_3' k_x k_y$	0	$-i\frac{1}{\sqrt{2}}Pk_-$	0
			$\varepsilon_{v0}-\frac{1}{2}\gamma_1' k^2+\frac{1}{2}\gamma_2'(k_x^2+k_y^2-2k_z^2)$	0	$-\frac{\sqrt{3}}{2}\gamma_2'(k_x^2-k_y^2)+i\sqrt{3}\gamma_3' k_x k_y$	$i\frac{\sqrt{2}}{\sqrt{3}}Pk_z$	$-i\frac{1}{\sqrt{6}}Pk_-$
				$\varepsilon_{v0}-\frac{1}{2}\gamma_1' k^2+\frac{1}{2}\gamma_2'(k_x^2+k_y^2-2k_z^2)$	$-\sqrt{3}\gamma_3' k_z k_-$	$-i\frac{1}{\sqrt{6}}Pk_+$	$-i\frac{\sqrt{2}}{\sqrt{3}}Pk_z$
					$\varepsilon_{v0}-\frac{1}{2}\gamma_1' k^2-\frac{1}{2}\gamma_2'(k_x^2+k_y^2-2k_z^2)$	0	$-i\frac{1}{\sqrt{2}}Pk_+$
						$\varepsilon_{c0}+\gamma_c' k^2$	0
							$\varepsilon_{c0}+\gamma_c' k^2$

TABLE III. Parameters for GaAs and InSb, entering the $\mathbf{k}\cdot\mathbf{p}$ matrices. The values for the Luttinger parameters (LP) γ_i' for the 8×8 $\mathbf{k}\cdot\mathbf{p}$ model follow from those for the usual values γ_i by taking into account the remote bands via the Löwdin renormalization as presented by Cardona *et al.* (Ref. 15).

Parameter		GaAs	InSb
a_0(Å)	lattice constant	5.65325 [a]	6.479 [b]
$m_c^\star$ (a.u.)		0.0665 [a]	0.014 [b]
E_0 (eV) [b]	$\varepsilon_{\Gamma_6^c}-\varepsilon_{\Gamma_8^v}$	1.519	0.235
Δ_0 (eV) [b]	$\varepsilon_{\Gamma_8^v}-\varepsilon_{\Gamma_7^v}$	0.340	0.803
P (a.u.) [b]	$\langle\Gamma_{7,8,x}^v\|p_x\|\Gamma_6^c\rangle$	0.692	0.661
γ_1 [b]	LP	6.85	40.1
γ_2 [b]	LP	2.10	18.1
γ_3 [b]	LP	2.90	9.2
γ_c	LP $[=1/(2m_c^\star)]$	7.519	35.71
γ_1'	LP	1.13	6.37
γ_2'	LP	−0.759	1.24
γ_3'	LP	0.0405	2.34
γ_c'	LP	−0.538	−1.83

[a]From Ref. 34.
[b]From Ref. 15.

It can be shown that the eigenstates obtained with the set of linear independent initial conditions (8) are orthonormal (see Appendix B). Therefore, the absorption coefficient can be calculated directly from these states.

Equation (5) reveals the main advantages of solving the FK problem in $\mathbf{k}$ space instead of real space. First the eigenstate problem has been reduced from a second- to a first-order differential equation. Transforming Eq. (5) into the integral equation (7) implies the second advantage: improper eigenstates will not occur in the solution, since the Fourier transform applied during the transformation from real space to $\mathbf{k}$ space implicitly suppresses non-normalizable solutions. Finally, it can easily be seen that states of different energies are related to each other via

$$c_{n,\mathbf{k}_\perp}^{F,\varepsilon+\Delta\varepsilon}(k_\parallel)=c_{n,\mathbf{k}_\perp}^{F,\varepsilon}(k_\parallel)e^{-i(\Delta\varepsilon/eF)k_\parallel}. \tag{9}$$

Thus it is sufficient to solve Eq. (5) for one energy ε_0, which is chosen in the center of the gap in order to keep the oscillations of all spinor components a minimum. States of different energies are derived via Eq. (9).

B. The absorption coefficient

Inserting the states obtained via Eq. (5) into the well-known formula for the absorption coefficient for direct semiconductors in the dipole approximation (cf., e.g., Ref. 17) leads to

$$\alpha(\hbar\omega)=\frac{e^2}{4\pi m^2 c}\frac{1}{\omega n(\omega)}\frac{1}{eF}\sum_{i,f}\int d\mathbf{k}_\perp\Big|\sum_{n_i,n_f}\int_{\Delta_\parallel}dk_\parallel c_{\mathbf{k}_\perp n_f\varepsilon_0}^{*(f)}(k_\parallel)c_{\mathbf{k}_\perp n_i\varepsilon_0}^{(i)}(k_\parallel)e^{-i(\hbar\omega/eF)k_\parallel}\hat{\mathbf{e}}\cdot[\hbar\mathbf{k}\delta_{n_in_f}+\mathbf{P}_{n_fn_i}]\Big|^2, \tag{10}$$

where the momentum of the photon has been neglected. i and f both include states, the initial conditions of which correspond to valence-band *and* conduction-band states. As is obvious from the real-space band diagram (Fig. 1) transitions from conduction-band states to valence-band states of higher energy become possible when an electric field is applied. Roughly speaking, conduction-band states can be occupied even at zero excitation intensity since every eigenstate of the system is an admixture of conduction- and valence-band states. However, the probability for this process is very small. Neglecting them did not visibly change our absorption spectra.

$n(\omega)$ is the index of refraction (values from Ref. 18). The absorption coefficient includes interband transitions via the term $\mathbf{P}_{n_fn_i}$ as well as intraband transitions via the term $\hbar\mathbf{k}\delta_{n_in_f}$. Calculations including the second term have confirmed the assumption expressed previously by some authors (see, e.g., Ref. 13) that the latter kind of transitions can be neglected. They lead to minimum changes of α only for $\hbar\omega$ high above E_g (of the order of 1%) and are thus omitted in the calculations presented here.

The polarization dependence enters through the bulk momentum matrix elements

$$\mathbf{P}_{n_fn_i}=\langle u_{n_f\mathbf{0}}|\mathbf{p}|u_{n_i\mathbf{0}}\rangle. \tag{11}$$

There are two choices for the polarization vector being of special importance: in transverse magnetic (TM) polarization $\hat{\mathbf{e}}$ is parallel to the static field and in transverse electric (TE) polarization it is orthogonal to the field. For these orientations the transitions from different valence bands are weighted with different matrix elements $\hat{\mathbf{e}}\cdot\mathbf{P}_{n_fn_i}$. The $\mathbf{P}_{n_fn_i}$ for the functions $u_{n\mathbf{0}}$ of Table I are given in Table IV.

C. Tools for the numerical realization

In spite of the simplicity of Eq. (5), the numerical evaluation requires a considerable amount of computing time. To reduce it, the full symmetry of the crystal has to be exploited. Each symmetry operation of the lattice has an analog in the coupled spin, real, and $\mathbf{k}$-space representation used in the $\mathbf{k}\cdot\mathbf{p}$ expansion (see, e.g., Jones, Ref. 19 and references

TABLE IV. Matrix elements $\mathbf{P}_{n_f n_i}$ for the functions $u_{n\mathbf{0}}$ of Table I. $P=i\hbar/m\langle j|p_j|s\rangle$ for $j\in\{x,y,z\}$, $P_z=(0,0,P)$, and $P_\pm=(P,\pm iP,0)$.

	$\lvert\frac{1}{2},\frac{1}{2}\rangle$	$\lvert\frac{1}{2},-\frac{1}{2}\rangle$	$\lvert\frac{3}{2},\frac{3}{2}\rangle$	$\lvert\frac{3}{2},\frac{1}{2}\rangle$	$\lvert\frac{3}{2},-\frac{1}{2}\rangle$	$\lvert\frac{3}{2},-\frac{3}{2}\rangle$
$\langle s\lvert\uparrow$	$\frac{-i}{\sqrt{3}}P_z$	$\frac{-i}{\sqrt{3}}P_-$	$\frac{i}{\sqrt{2}}P_+$	$-i\sqrt{\frac{2}{3}}P_z$	$\frac{i}{\sqrt{6}}P_-$	0
$\langle s\lvert\downarrow$	$\frac{-i}{\sqrt{3}}P_+$	$\frac{i}{\sqrt{3}}P_z$	0	$\frac{i}{\sqrt{6}}P_+$	$i\sqrt{\frac{2}{3}}P_z$	$\frac{i}{\sqrt{2}}P_-$

therein), leaving the matrix $H^{\mathbf{k}\cdot\mathbf{p}}$ invariant. Since the functions $u_{n\mathbf{0}}$ are chosen to have the symmetry of the crystal, operations that leave the plane perpendicular to the field invariant do so also for the whole Eq. (5). Therefore, it is sufficient to calculate states for the $\mathbf{k}_\perp$ values of one invariant sector of this plane. The numerical effort can thus be reduced by a factor of 4 in the zinc-blende structure, and in the diamond-structure even by a factor of 8 if the field is parallel to one of the main crystal axes.[20] For this reason we approximated the GaAs structure by the diamond structure neglecting the small-**k** linear terms in the **k·p** Hamiltonian. Calculations of the dispersions for both structures confirmed that this causes negligible changes in the absorption only, which are especially irrelevant for the effects on which we have focused our attention.

Since the system is invariant under time inversion it is sufficient to calculate the states $\mathbf{c}^{(m)}$ for half the initial conditions m. The other states can be derived from these by simple exchange relations and complex conjugation.

A numerical problem is the noise in the absorption spectra caused by the arbitrary upper integration limit in the determination of the FK eigenstates. Although the maximum values of $k_\parallel$ we used are in a region where the $c_{n\mathbf{k}_\perp}(\mathbf{k}_\parallel)$ are already oscillating so rapidly that destructive interference between these parts of the wave functions makes their contribution to the overlap very small, unfinished oscillation periods at the edge of the integration interval result in nonvanishing fluctuating contributions. This effect produces an error in the overlap that is detrimental to the calculations in the range of very-low-α values. In order to reduce this error we introduce a damping function $d(\mathbf{k})$ in the overlap. This function has to be chosen such that it does not affect the parts of the states corresponding to low values of $k_\parallel$, but, nevertheless, still drastically suppresses the last oscillation. We obtained the best results with

$$d(\mathbf{k})=\exp\left[-d_0\frac{|\mathbf{k}|^j}{|\mathbf{k}_{\max}|^j}\right] \tag{12}$$

and $j=4$. $|\mathbf{k}_{\max}|$ is the maximum $|\mathbf{k}|$ occurring in the calculations. For higher values of j the damping sets in too late, for lower values it is too early. For $j=4$, $d_0=4$ turned out to be the best choice. The effect of this damping is not visible for photon energies above E_g, but improved the accuracy of the spectra by almost two orders of magnitude below the band gap (thus we reach an accuracy in α of more than 10^4). Such a damping function is not just an artifical tool for improving the numerics, but also corresponds to **k**-dependent broadening mechanisms present in the real crystal.

III. RESULTS

In the following, results obtained for GaAs as one of the most common III-V semiconductors will be used to demonstrate the main features of the FK absorption in our realistic band-structure model in comparison with calculations based on the EMA. Additional results are given for InSb as an example for a low-gap semiconductor, in which band coupling is much more pronounced. The field is assumed to be in the [001] direction, which is the typical case for epitaxially grown *p-i-n* junctions. The results will be discussed for a set of field values between $F=31.25$ and $F=250$ kV/cm with an increase of a factor of 2 from each one to the next value. In this way, they cover the range of low fields to a value somewhat below the breakthrough field.

A. The k·p models used for the calculations

A number of different **k·p** models are used for the FK calculations in order to reveal the different features of the band structure with respect to their influence on the characteristics of the absorption spectra. The considerations will be restricted to the energy range around the fundamental gap energy. Thus the split-off (SO) holes can be neglected if they are decoupled from the other bands in the respective model. The models are the following.

1. The fully coupled 8×8 k·p model

This model is the most realistic available description of the band-structure effects in the relevant k range. It includes the Γ_6^c, Γ_7^v, and Γ_8^v bands in the vicinity of the fundamental gap and the full range of renormalized interaction terms between them. The FK absorption spectra obtained in this model are considered to be exact within the single-particle approximation.

2. The Luttinger model

This model consists of the Γ_6^c conduction bands and the Γ_8^v valence bands, described by the Luttinger Hamiltonian.[21,22] Here the coupling between the heavy-hole (HH) and light-hole (lh) bands is fully included up to second order in k, but the interaction between the conduction and the valence bands and the interaction between the SO valence band and the hh/lh valence bands are neglected. Therefore, the band dispersions are purely parabolic and a comparison with the 8×8 **k·p** model reveals the importance of nonparabolicity effects.

3. A nonparabolic EMA model

In this model, the Hamilton matrix $H^{\mathbf{k}\cdot\mathbf{p}}_{n'n}(k_\parallel,\mathbf{k}_\perp)$ appearing in Eq. (5) is diagonal, the diagonal elements containing the dispersion relations $\varepsilon_n(k_\parallel,\mathbf{k}_\perp)$ of the bands as obtained from a diagonalization of the zero-field $\mathbf{k}\cdot\mathbf{p}$ Hamiltonian. Equations (5) are now decoupled and can be integrated analytically, yielding

$$c^{F,\varepsilon}_{n,\mathbf{k}_\perp}(k_\parallel)=c^{F,\varepsilon}_{n,\mathbf{k}_\perp}(0)\exp\left\{\frac{i}{eF}\int_0^{k_\parallel}[\varepsilon_n(k'_\parallel,\mathbf{k}_\perp)-\varepsilon]dk'_\parallel\right\}. \quad (13)$$

Furthermore, the momentum matrix elements $|\hat{\mathbf{e}}\mathbf{P}_{n_f n_i}|^2$ in Eq. (10) are replaced by a k-independent angular average, giving

$$|\hat{\mathbf{e}}\mathbf{P}_{c,\mathrm{hh}}|^2=|\hat{\mathbf{e}}\mathbf{P}_{c,\mathrm{lh}}|^2=\tfrac{2}{3}P^2, \quad (14)$$

using the results of Yamanishi and Suemune.[23] The above representation can be obtained from Eq. (5) by a unitary transformation if one neglects the interband matrix elements of the electric field. In this way it contains the band nonparabolicity exactly on the level of the dispersion relations, but does not account for the explicit band coupling through the field. By the use of the averaged momentum matrix elements polarization effects are suppressed. In the zero-field case the calculated absorption is proportional to the combined density of states of electrons and holes, which deviates slightly from the real single-particle absorption because the $|\mathbf{k}|$ dependence of the momentum matrix elements is neglected. This model is expected to be good for weak fields and to account well for the influence of band nonparabolicity on the period of the FK oscillations and the decay constant of the absorption tail.

4. The two-dimensional (2D) diagonal approximation (two-dimensional EMA)

This model consist of the diagonal parts of the Γ_6^c conduction bands (CB's) and the Γ_8^v valence bands (VB's). In this model the hh and lh states are decoupled, which becomes exact in the limit of vanishing in-plane $\mathbf{k}$ vector and zero CB-VB coupling. The electrons are characterized by an isotropic effective mass m_c^* the hole masses, however, have different components for the z direction ($m^*_{\mathrm{hh/lh},\parallel}$) and the in-plane direction ($m^*_{\mathrm{hh/lh},\perp}$):

$$m^*_{\mathrm{hh},\parallel}=\frac{m}{\gamma_1-2\gamma_2},\quad m^*_{\mathrm{hh},\perp}=\frac{m}{\gamma_1+\gamma_2}, \quad (15)$$

$$m^*_{\mathrm{lh},\parallel}=\frac{m}{\gamma_1+2\gamma_2},\quad m^*_{\mathrm{lh},\perp}=\frac{m}{\gamma_1-\gamma_2}. \quad (16)$$

The momentum matrix elements, contained in Table IV, are polarization dependent:

$$|\hat{\mathbf{e}}\mathbf{p}_{c,\mathrm{hh}}|^2=(e_x^2+e_y^2)P^2, \quad (17)$$

$$|\hat{\mathbf{e}}\mathbf{p}_{c,\mathrm{lh}}|^2=[\tfrac{1}{3}(e_x^2+e_y^2)+\tfrac{4}{3}e_z^2]P^2. \quad (18)$$

Therefore, this model yields a difference in the absorption for radiation polarized in the x-y and the z direction, which is not allowed for the zero field due to the isotropy of the crystal. Although the zero-field limit is inconsistent, it will be shown that the polarization dependence of the absorption tail below the band gap should be described correctly by this model. Furthermore, it contains more realistic hh and lh densities of states than the EMA models A and B (see below), since it includes the mass reversal effect. This model is identical to the widely used EMA for two-dimensional systems such as quantum-well structures.

5. Two EMA models reflecting the properties of three-dimensional systems (3D-diagonal approximation)

In both models the conduction-band dispersions are characterized by a constant effective mass m_c^*. In the one model (EMA A) the holes are described by keeping only the s-like part of the diagonal terms of the Luttinger Hamiltonian and removing all off-diagonal terms.[24] Then, the holes are described by a common isotropic effective mass

$$m_v^*=m^*_{\mathrm{hh}}=m^*_{\mathrm{lh}}=\frac{m}{\gamma_1} \quad (19)$$

for both the light and heavy holes. For the other model (EMA B) the spherical approximation[25] is applied, giving isotropic effective hole masses

$$m^*_{\mathrm{hh}}=\frac{m}{\gamma_1-2\gamma_{\mathrm{sph}}}, \quad (20)$$

$$m^*_{\mathrm{lh}}=\frac{m}{\gamma_1+2\gamma_{\mathrm{sph}}}, \quad (21)$$

with $\gamma_{\mathrm{sph}}=\frac{1}{5}(2\gamma_2+3\gamma_3)\approx\gamma_2$. In the expressions of the absorption the averaged momentum matrix elements of Eq. (14) are used. Both models do not account for any of the band structure effects and cannot describe the polarization dependence of the absorption. Thus a comparison with the above models can reveal how important these effects are for the FK absorption.

6. An EMA model that totally neglects any hole dispersion ($\mu_{cv}=m_c^*$)

In this model the momentum matrix elements are chosen as in Eq. (14).

B. Zero-field absorption: Density-of-states effects

One of the most basic improvements of refined $\mathbf{k}\cdot\mathbf{p}$ models in comparison with the EMA are quantitative changes of the absorption coefficient due to both changes in the combined density of states (CDOS) of electrons and holes and the bulk momentum matrix elements. In order to investigate this effect in more detail, the dispersion relations of the relevant bands of GaAs, calculated with different models, are plotted in Fig. 2. In a small energy range around the band gap ($\hbar\omega-E_g<300$ meV, corresponding to $k<0.1\pi/a_0$), the deviations between the exact dispersions and the EMA seem to be comparably small, except for the strong warping of the hh band. However, it is difficult to estimate the effect on the CDOS quantitatively from the dispersion relations. It is interesting to note that the CB-VB coupling, which is only present in the 8×8 $\mathbf{k}\cdot\mathbf{p}$ model, even tends to decrease the hh DOS in comparison with the Luttinger model. However, due to the band warping it remains higher than in the EMA.

Figure 3 shows single-particle zero-field absorption spectra calculated with the full 8×8 $\mathbf{k}\cdot\mathbf{p}$ model, the nonpara-

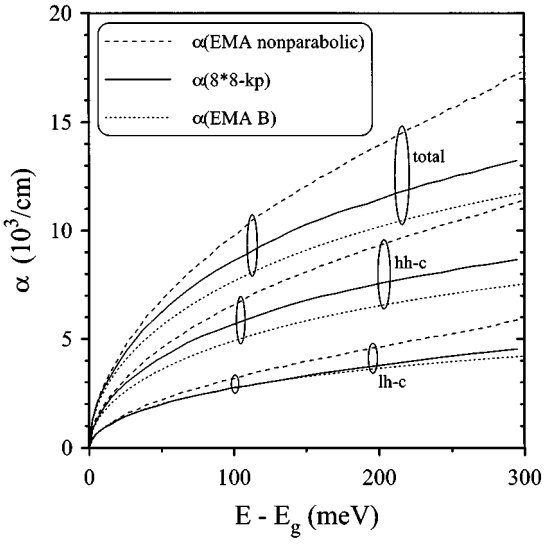

FIG. 3. Zero-field single-particle absorption of GaAs, calculated within the 8×8 **k·p** model and the EMA B.

bolic EMA, and the EMA B. For the nonparabolic EMA and the EMA B the absorption is (neglecting the contribution of the SO holes)

$$\alpha(\omega)\propto\frac{1}{\omega}\sum_{v=\mathrm{hh,lh}}\frac{2}{3}P^2D_{cv}(\hbar\omega), \tag{22}$$

where $D_{cv}(\hbar\omega)$ is the CDOS for electrons and holes in the respective model. Thus the absorption coefficient is directly proportional to the CDOS, apart from an additional factor $1/\omega$.

The values obtained with the nonparabolic EMA, which reflect the CDOS of the full 8×8 **k·p** Hamiltonian, are considerably enhanced in comparison with the EMA B, the amount increasing with increasing energy. The enhancement factor reaches a value of approximately 1.5 at an energy of 300 meV above the band-gap energy and is nearly the same for the heavy holes and the light holes, indicating that it mainly results from the nonparabolicity of the conduction band.

The situation is different for the exactly calculated absorption spectra, including the band mixing in the momentum matrix elements. Here the expression for the absorption coefficient in the 8×8 **k·p** model becomes

$$\alpha(\omega)\propto\frac{1}{\omega}\sum_{v=\mathrm{hh,lh}}\overline{|p_{cv}|^2}D_{cv}(\hbar\omega), \tag{23}$$

where $\overline{|p_{cv}|^2}$ is an average over the momentum matrix elements of all transitions at an energy $\hbar\omega$. $\overline{|p_{cv}|^2}$ becomes equal to $\frac{2}{3}P^2$ for $\hbar\omega\rightarrow E_g$, but deviates from this value for increasing energy. The absorption calculated for the 8×8 **k·p** model is still increased in comparison to the EMA B, but the enhancement is much less than for the nonparabolic EMA. This is a result of states mixing in the momentum matrix elements. The CB Bloch states gain contributions from the Γ-point VB states and vice versa for the VB states. In total, however, they have to remain normalized. The momentum matrix elements now contain contributions of the

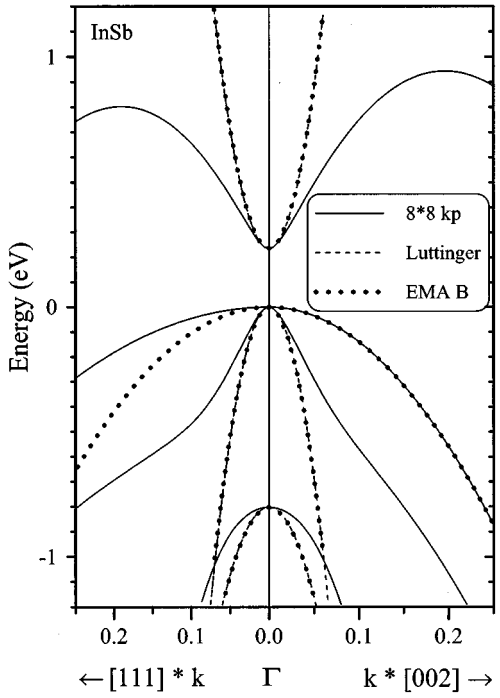

FIG. 4. Conduction- and valence-band dispersions of InSb, calculated within the 8×8 **k·p** model, the Luttinger model, and the EMA B.

type $\langle\phi_{c0}|\hat{\vec{p}}|\phi_{c0}\rangle$ and $\langle\phi_{v0}|\hat{\vec{p}}|\phi_{v0}\rangle$ (c and v stand for the possible CB and VB orbitals), which are zero and reduce their total average squares below $\frac{2}{3}P^2$. This property is responsible for the fact that the exact absorption curves are only slightly enhanced in comparison to the EMA B.

In order to see the nonparabolicity effects more clearly, InSb has been chosen as an example for a low-gap material ($E_g=0.235$eV for $T=0$ K) with a much more pronounced band coupling. Here the deviations of the realistic band structure from the EMA are large (Fig. 4). Note that the coupling of heavy holes to the split-off holes is so small (the

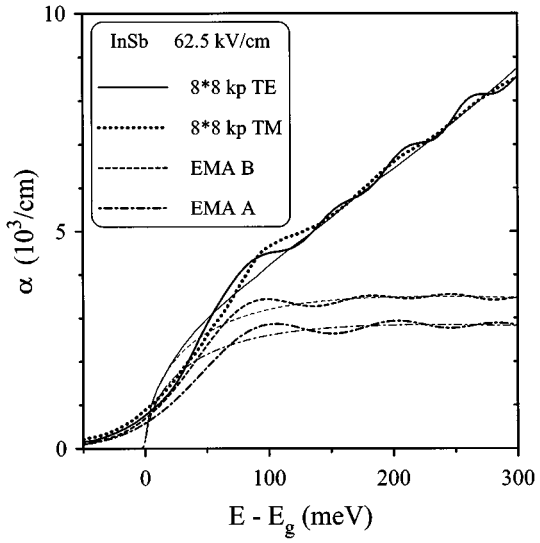

FIG. 5. Zero-field and Franz-Keldysh absorption spectra of InSb, calculated within the 8×8 **k·p** model and the EMA models.

Γ_7^v-Γ_8^v splitting is $\Delta_0 = 0.803$ eV) that the $\mathbf{k}\cdot\mathbf{p}$ model and the Luttinger model are in full agreement for the hh dispersions. The zero-field absorption spectra are included in Fig. 5. There is a steep increase of the absorption above the band gap in the 8×8 $\mathbf{k}\cdot\mathbf{p}$ model, whereas the EMA absorption curves even obtain a negative slope, resulting from the $1/\omega$ behavior of Eq. (22), the decrease of which exceeds the increase of the square-root-shaped CDOS.

C. Comparison with EMA spectra

For the parabolic EMA models the expressions (13) and (10) can be evaluated analytically, yielding[3]

$$\alpha(\omega,F)=\frac{2\pi e^2}{m^2 c\omega n(\omega)\hbar^2}eF \times\sum_{v=\{\mathrm{rmhh,lh}}\frac{\mu_{cv,\perp}}{\hbar\theta_{cv}}|\hat{\mathbf{e}}\mathbf{p}_{cv}|^2\{[\mathrm{Ai}'(x_{cv})]^2 -x_{cv}\mathrm{Ai}(x_{cv})\}, \tag{24}$$

with

$$\hbar\theta_{cv}=\left[\frac{(eF\hbar)^2}{2\mu_{cv,\parallel}}\right]^{1/3}, \tag{25}$$

$$x_{cv}=\frac{E_g-\hbar\omega}{\hbar\theta_{cv}}. \tag{26}$$

The energy dependence of the structures in the absorption spectra is therefore determined by the Airy function $\mathrm{Ai}(x)$ and its derivative [the smoothly varying factor $1/\omega n(\omega)$ can be neglected], depending on the dimensionless variable x_{cv} . x_{cv} is determined by the electric field F and the reduced effective mass of electrons and holes $\mu_{cv,\parallel}$ such that the FK absorption tail and the period of the FK oscillations grow when the field is increased or the effective mass reduced. The total absorption is the sum of a hh and a lh part, the contribution of each depending mainly on the individual values of $|\hat{\mathbf{e}}\mathbf{p}_{cv}|^2$.

In Fig. 6, FK spectra for GaAs at two different values of the electric field are shown. The spectra using the 8×8 $\mathbf{k}\cdot\mathbf{p}$ model have been calculated for the incident radiation polarized parallel (TM) and perpendicular (TE) to the static electric field. The EMA models cannot distinguish between the polarization directions.

The band coupling does not alter the basic characteristics of the FK effect, i.e., an exponentially decreasing absorption tail below the band-gap energy and oscillations around the zero-field absorption above. The fact that the FK absorption curves in the 8×8 $\mathbf{k}\cdot\mathbf{p}$ model seem to lie above the zero-field absorption for high energies is due to numerical errors. A couple of features can be recognized in the FK absorption spectra, which will be discussed in detail in the following sections.

(i) A clear difference is observed between TE- and TM-polarized absorption spectra, both with respect to the magnitude of the absorption tail and the period of the FK oscillations. In addition, a beating of the FK oscillations occurs for the TE polarization (between the third and the fourth FK oscillation maximum in the $F=62.5$ kVcm spectrum), which is absent for the TM polarization. It results from the interference of the hh-CB and lh-CB contributions to the absorption (the position of a hh-c oscillation minimum coincides with a lh-CB maximum) and is also present in the EMA B, whereas the EMA A fails to reproduce this feature, as it contains only one hole type.

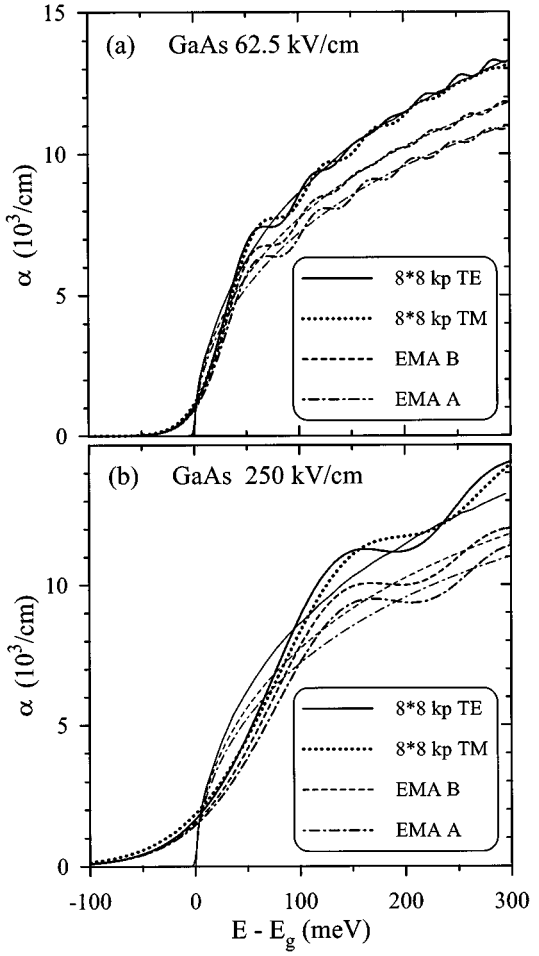

FIG. 6. Franz-Keldysh absorption spectra of GaAs for two values of the electric field, calculated within the 8×8 $\mathbf{k}\cdot\mathbf{p}$ model and the EMA models. For comparison the zero-field spectra are included as well.

(ii) The FK oscillation periods in the 8×8 $\mathbf{k}\cdot\mathbf{p}$ model deviate from the EMA models. This effect can mainly be attributed to band nonparabolicity and is important for the interpretation and possible experimental evaluation of data such as electric fields and effective masses from the absorption spectra. In general, the oscillation period is reduced when the reduced effective mass is increased. This is a common property of the wave functions and the absorption spectra. The oscillation periods in the EMA model A are larger than in model B, since the averaged reduced effective mass of model A is smaller than the hh-CB mass of model B, the contribution of which dominates the absorption in model B.

Similar to the CDOS effects, the above effects are much

more prominent in the low-gap semiconductor InSb (Fig. 5). The comparative weakness of the band coupling effects in large-gap semiconductors such as GaAs is responsible for the EMA theories to be a good approximation, but they clearly fail in the case of low-gap semiconductors such as InSb.

D. Polarization dependence of the absorption

The origin of the polarization dependence of the FK absorption spectra can be understood in analogy to quasi-2D systems by the anisotropy of the hh and lh orbitals, oriented along the electric field axis, which is the direction in which the cubic symmetry of the crystal is broken. In quantum-well structures the quantum-well potential leads to a splitting of the hh and the lh states. If the z direction is chosen to be the growth direction and the in-plane wa vevector $\mathbf{k}_\perp$ equal to zero, the hh and lh states can mostly precisely be described by the functions contained in Table I. Thus each subband contributes a very simple and pronounced polarization behavior at the subband edge, which reflects the angular dependence of the basis states and can be calculated using Eqs. (17) and (18). This is valid as long as the coupling between hh and lh subbands is weak, i.e., the energy separation between the subbands larger than the $\mathbf{k}_\perp$-dependent off-diagonal terms in the $\mathbf{k}\cdot\mathbf{p}$ matrices.

For the bulk electroabsorption case, however, hh and lh states are degenerate for every value of the energy and every value of the in-plane $\mathbf{k}$ vector. Consequently, contributions of both hole types are present at any point of the absorption spectrum. Moreover, the absorption at each value of the photon energy is, in principle, composed of contributions with arbitrary values of $\mathbf{k}_\perp$ since the energy spectrum is continuous and unbounded in both directions and an eigenstate exists for any value of $\mathbf{k}_\perp$. Therefore, the off-diagonal terms of the $\mathbf{k}\cdot\mathbf{p}$ matrices are always large and a decoupling of hh and lh states as obtained for $\mathbf{k}_\perp=\mathbf{0}$ in quantum-well structures does never occur. This makes the situation highly complex.

Practically, however, the range of relevant $\mathbf{k}_\perp$ vectors has an upper limit, as mentioned in Sec. II A. Here the consequences shall be dicussed in some more detail. An EMA picture will be used because it allows for a separation of the total energy into a component in the field direction ($\varepsilon_\parallel$) and the in-plane direction. If the total transition energy

$$\hbar\omega=\varepsilon_{c,\parallel}-\varepsilon_{v,\parallel}+\frac{\hbar^2k_\perp^2}{2m_{c,\perp}^*}+\frac{\hbar^2k_\perp^2}{2m_{v,\perp}^*}=\varepsilon_{c,\parallel}-\varepsilon_{v,\parallel}+\frac{\hbar^2k_\perp^2}{2\mu_{cv,\perp}} \tag{27}$$

is kept constant and the value of $\mathbf{k}_\perp$ increased, $\varepsilon_{c,\parallel}-\varepsilon_{v,\parallel}$ has to decrease. If it falls below the band gap energy E_g, i.e.,

$$\frac{\hbar^2k_\perp^2}{2\mu_{cv,\perp}}>\hbar\omega-E_g, \tag{28}$$

the contributions to the absorption will decay rapidly since they correspond to pairs of electron and hole wave functions, which only overlap in their tail regions. These considerations remain valid if the full band coupling is included.

Equation (28) is always fulfilled for photon energies below the band-gap energy E_g. In this case only a small range of $\mathbf{k}_\perp$ values around $\mathbf{k}_\perp=\mathbf{0}$ contributes significantly to the absorption and the off-diagonal coupling between the spinor components of the corresponding states is small. Therefore, the application of the 2D diagonal approximation should be satisfied. This limit has been discussed by Keldysh *et al.*[12] before, who obtained the same results. In any other case, however, the full coupling between the bands has to be included.

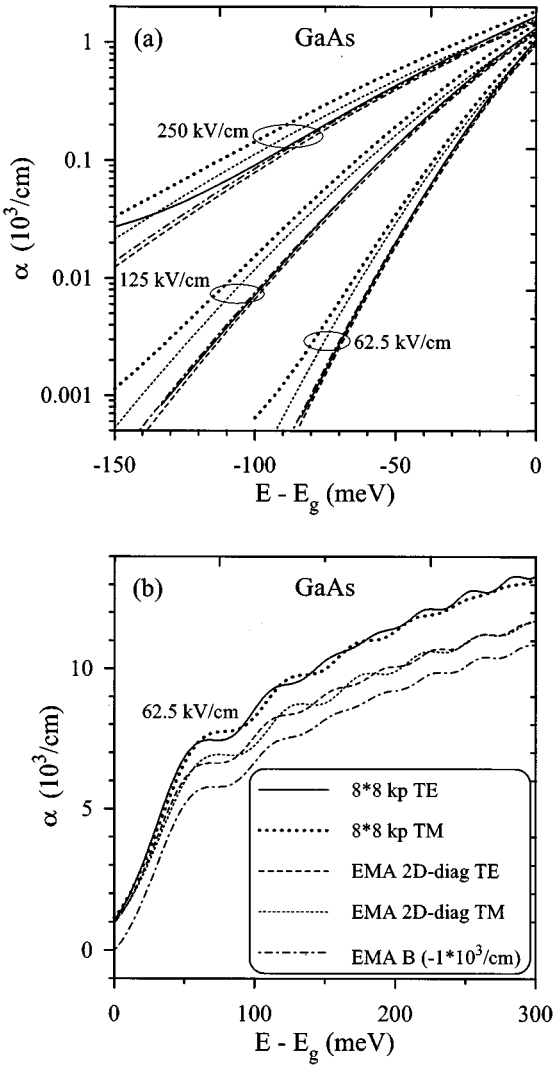

FIG. 7. Franz-Keldysh absorption of GaAs in TE and TM polarization, calculated with different models. (a) Absorption tail below the band-gap energy and (b) FK oscillations above the band-gap energy.

Figure 7(a) shows the FK absorption tails below the band-gap energy in a logarithmic scale for various values of the electric field, calculated with different models. Here TE denotes a component with the polarization perpendicular to the field, i.e., in the x direction; for TM the polarization is parallel to the field. The TM absorption exceeds the TE absorption in the whole energy range below the band gap, in both the 8×8 $\mathbf{k}\cdot\mathbf{p}$ model and the 2D diagonal approximation. This can be easily understood in the 2D diagonal approximation. Using Eqs. (17) and (18) it is possible to decompose the total absorption into its hh-CB and lh-CB contributions, writing, for TE and TM absorption, respectively,

$$\alpha_{\mathrm{TE}}(\omega)=P^2\alpha_{\mathrm{hh}}(\omega)+\tfrac{1}{3}P^2\alpha_{\mathrm{lh}}(\omega), \tag{29}$$

$$\alpha_{\mathrm{TM}}(\omega)=\tfrac{4}{3}P^2\alpha_{\mathrm{lh}}(\omega). \tag{30}$$

α_{hh} and α_{lh} differ from each other by the square of the envelope function overlaps with respect to the field direction and the CDOS in the perpendicular direction. In the 2D diagonal approximation the lh-CB CDOS is larger than the hh-*c* CDOS due to the mass-reversal effect. Furthermore, the tunneling tail of the hh envelopes into the band-gap region decays more rapidly than that of the lh envelopes, yielding smaller overlaps with the electron envelopes for photon energies below the band-gap energy. Both cause α_{lh} to be larger than α_{hh} and the ratio grows with decreasing photon energy. Thus the TM absorption, which entirely consists of lh-CB contributions, exceeds the TE absorption, which is dominated by hh-CB contributions.

In Fig. 7(a) one realizes that the agreement between the 8×8 $\mathbf{k}\cdot\mathbf{p}$ model and the 2D diagonal approximation is nearly perfect with respect to the energy dependence of the absorption. The total values differ by a small and nearly constant factor, resulting from the higher in-plane CDOS of the 8×8 $\mathbf{k}\cdot\mathbf{p}$ model due to band warping and band nonparabolicity. The deviations for small photon energies are due to numerical errors. There is also good agreement of the EMA model *B* with the TE absorption of the 8×8 $\mathbf{k}\cdot\mathbf{p}$ model, but the absorption decay with the energy is slightly smaller. This results from the fact that the contribution of lh-*c* transitions in comparison to the hh-CB transitions is too large in the EMA *B*.

Figure 7(b) contains a comparison of TE and TM absorption spectra above the band-gap energy. Although the 2D diagonal approximation should not be valid in this energy range, results are given for comparison. Surprisingly, the agreement with the 8×8 $\mathbf{k}\cdot\mathbf{p}$ model is rather good. Even the magnitudes of TE and TM absorption almost seem to coincide, although this is not necessary in the 2D diagonal approximation. Indeed, the calculation of the zero-field absorption in this model accidentally yields TE and TM values that differ by less than 1%, but this is only possible as long as the low CB mass dominates the reduced effective mass.

Nevertheless, the system behaves, as if hh-CB and lh-CB transitions were nearly decoupled. The width of the oscillation periods in TE polarization is smaller than in TM polarization because the absorption is dominated by the hh-CB contributions, which have shorter oscillation periods than the lh-CB contributions. Additionally, a beating of the hh-CB and the lh-CB contributions occurs in the TE polarization but not in the TM polarization, which has already been discussed in Sec. III C. Apart from slight deviations of the FK oscillation periods, which will be discussed in Sec. III E, the band coupling manifests only in an increased damping of the higher FK oscillations in the TM mode and a reduced damping in the TE mode.

The difference between the TE and the TM absorption for energies below the band gap has been observed in several experiments.[26–28] Recently the polarization characteristics of the FK absorption has also been investigated above the band-gap energy in experiments on low-temperature grown GaAs.[29] Owing to the high breakthrough fields in this material, high voltages could be applied between lateral contacts, allowing for polarization-dependent transmission measurements with light incidence perpendicular to the sample surface. As predicted by theory, a comparison of the TM with the TE absorption yielded higher absorption values below the band-gap energy and larger FK oscillation widths above. Unfortunately, more than one FK oscillation could not be resolved due to broadening and field inhomogeneity, so that the beating of the hh-CB and lh-CB contributions was not visible. It has, however, been observed in many photoreflectance experiments, e.g., in Refs. 30 and 31.

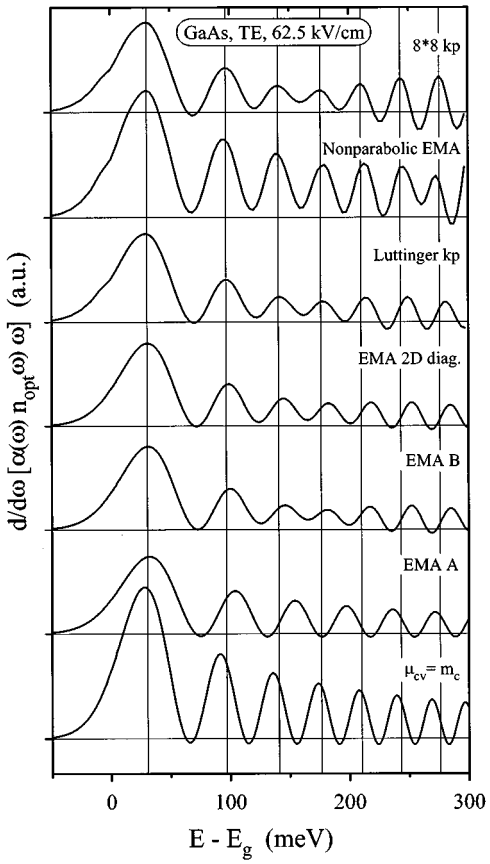

FIG. 8. Derivative of the Franz-Keldysh absorption of GaAs with respect to the photon energy, calculated for several models. The vertical lines mark the positions of the oscillation maxima in the 8×8 $\mathbf{k}\cdot\mathbf{p}$ model.

E. Band nonparabolicity effects

Apart from the density of states, which has been discussed in Sec. III B, the band coupling also affects the dynamics of the carriers, i.e., the shape and, in particular, the oscillation frequencies of the wave functions. The latter is closely related to the period of the FK oscillations in the electroabsorption spectra, which consequently should be an indicator for this effect.

To estimate its importance and its consequences, the FK oscillations obtained within the various models are compared. For this reason, the derivatives of the absorption with respect to the photon energy are shown for the TE mode of GaAs at $F=62.5$ kV/cm in Fig. 8.

Each of the models leads to its own line shapes, but there are a couple of common characteristics related to the properties of the band structure. First, the total values of the derivatives do not differ very much since the absorption values

are rather similar (cf. Fig. 7). This would be different in the low-gap material InSb, where the models involving band coupling strongly deviate from the EMA models. The nonparabolic EMA and the EMA neglecting the hole dispersion yield higher values of the absorption and its derivative because the former does not include the decreased values of the momentum matrix element resulting from CB-VB coupling and the latter overestimates the CDOS strongly.

In all models that explicitly include the heavy and light holes, there occurs a beating between the hh-CB and the lh-CB absorption contributions between the third and fourth oscillation periods. This behavior indicates that a decomposition of the absorption spectra into independent contributions from the light holes and heavy holes is not too far from reality. However, the magnitude of the oscillation interference differs strongly between the various models. It is nearly equivalent in the 8×8 $\mathbf{k}\cdot\mathbf{p}$ model and the Luttinger model, which shows that the hh-lh mixing only slightly depends on higher-order terms of the CB-VB coupling (up to second order in $\mathbf{k}$ it is already contained in the renormalized Luttinger Hamiltonian). If the coupled-band models are compared to the EMA models, an interesting result is obtained. The beating is more pronounced than in the 2D diagonal approximation, but less than in the 3D diagonal EMA *B*. This is again an indication that the system is between 2D and 3D character.

As discussed in Sec. III D, the periods of the FK oscillations are dominated by the hh contributions in the TE polarization and by the lh contributions in the TM polarization. An analysis of the oscillation periods, therefore, reveals the influence of band nonparabolicity on the respective absorption component. In Fig. 8 the position of the oscillation maxima obtained with the full 8×8 $\mathbf{k}\cdot\mathbf{p}$ Hamiltonian are marked by vertical lines. In general, deviations between the different models are small. Obviously, neglecting the explicit Γ_6-$\Gamma_{7/8}$ interaction, i.e., the CB-VB coupling (*Luttinger* $\mathbf{k}\cdot\mathbf{p}$), and any explicit interaction terms between the bands at all (2D diagonal EMA) leads to an enhancement of the oscillation periods by a similar amount. In both cases the reason for this behavior is decreasing effective masses: In the former case, the suppression of CB-VB coupling yields a reduced electron effective mass, in particular for higher energies, in the latter case, neglecting the off-diagonal terms of the Luttinger Hamiltonian leads to lower hh masses for $\mathbf{k}_\perp \neq \mathbf{0}$. It is interesting to note that the nonparabolic EMA results in almost the same FK oscillation periods as the exact model, in spite of the deviations in the oscillation amplitudes. However, it does not reproduce the interference between hh and lh FK oscillations properly since the hh contribution, which is strongly overestimated due to the large CDOS, completely dominates the spectra. This indicates that the oscillation periods mainly depend on the realistic shape of the $\varepsilon(k)$ dispersions, whereas the explicit consideration of the interband coupling terms mostly affects the FK oscillation amplitudes and the hh-lh interference. The results of the EMA *B* are nearly equivalent to those of the 2D diagonal approximation since hh and lh contribution only differ in magnitude due to different values of the momentum matrix element and the CDOS. In contrast, the EMA *A* yields oscillation periods that are clearly too large, resulting from the smaller values of the reduced effective masses. If, however, the reduced effective hole mass is assumed to be infinite, the FK oscillation widths are nearly equivalent to those of the 8×8 $\mathbf{k}\cdot\mathbf{p}$ model, although the positions of the maxima are slightly shifted to lower energies. This behavior, which was unexplained before, has already been observed by Rees in electroabsorption experiments on GaAs.[32]

The nonparabolicity effects can be expressed in terms of an electro-optic reduced effective mass. It will be defined by an evaluation of the FK oscillation extrema based on the EMA theory as given by expression (24). We will consider the derivative of the absorption with respect to the photon energy $(1/\hbar)(\partial\alpha/\partial\omega)$. If one neglects the factor $1/\omega n(\omega)$, the energy dependence of this expression is proportional to $\mathrm{Ai}^2(x_{cv})$. Assuming that either the hh or the lh contribution dominates, a single-band approximation is satisfied, and for this component the energies $\hbar\omega_n$ for the minima of the FK oscillations can approximately be related to the zeros of the Airy function $\mathrm{Ai}(x_n)$ by

$$x_n=\frac{E_g-\hbar\omega_n}{\hbar\theta_{cv}}. \tag{31}$$

Equation (31) can be solved for the reduced mass of electrons and holes

$$\mu_{cv}=\frac{1}{2}\frac{(eF\hbar)^2x_n^3}{(E_g-\hbar\omega_n)^3}. \tag{32}$$

Equation (32) can be used to define a reduced mass, which will be called the electro-optic mass. For a single-band EMA its value is, of course, constant and equal to the nominal value at the band-gap energy. In any other case, however, it will be energy dependent.

The reduced electrooptic effective mass will be compared with a reduced ''energy effective mass'' defined by

$$\mu^E_{cv,\parallel}(k_z)=\frac{\hbar^2k_z^2}{2[\varepsilon_{cv}(k_z)-E_g]}, \tag{33}$$

and a ''curvature effective mass'' given by

$$\mu^{\mathrm{curv}}_{cv,\parallel}(k_z)=\left[\frac{1}{\hbar^2}\frac{\partial^2\varepsilon_{cv}(k_z)}{\partial k_z^2}\right]^{-1}. \tag{34}$$

The former is obtained by writing the interband energy in the form of a free-particle dispersion

$$\varepsilon_{cv}(k_z)-E_g=\frac{\hbar^2k_z^2}{2\mu^E_{cv,\parallel}(k_z)}; \tag{35}$$

the latter describes the local properties of the interband dispersion around the point k_z in terms of a curvature parameter. In our context, both functions are defined for $\mathbf{k}_\perp=\mathbf{0}$.

In Fig. 9 the electro-optic mass as derived from the minima of the FK oscillations in the 8×8 $\mathbf{k}\cdot\mathbf{p}$ model for an electric field of $F=31.25$ kV/cm is shown by dots for the TE polarization and by asterisks for the TM polarization. For comparison, the reduced energy and curvature effective masses are included. Here the energy dependence of the masses has been transformed to the variable x_n by solving the equation

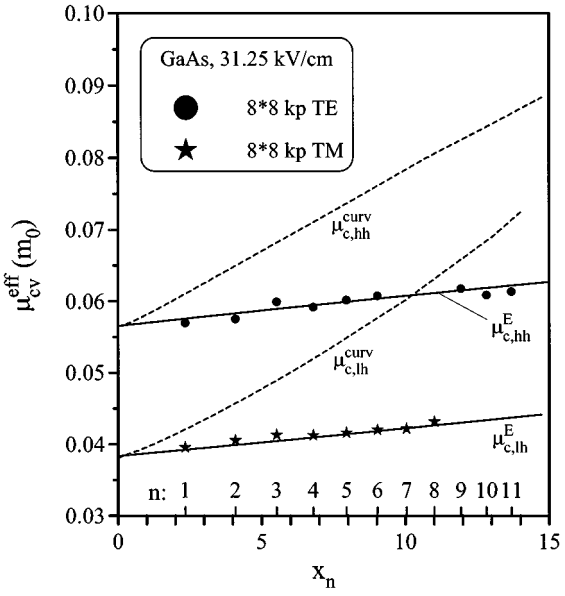

FIG. 9. Values of the energy-dependent electro-optic mass as obtained from the energy positions of the FK oscillation minima by the evaluation procedure described in the text.

$$x_n = \frac{E_g - \varepsilon_{cv}(k_\parallel)}{\hbar\,\theta_{cv}(k_\parallel)} \tag{36}$$

for $k_\parallel$ (in field direction) for each point x_n. Afterward the value obtained for $k_\parallel$ is used to calculate the effective masses from the exact dispersion relations obtained within the 8×8 $\mathbf{k}\cdot\mathbf{p}$ model. In the limit $x_n \to 0$, both energy and curvature effective masses reach the same values, which are given by the nominal values at the Γ point. Obviously the energy effective masses are in good agreement with the electro-optic masses rather than the curvature effective masses. Due to the dominance of either type of hole contribution the hh-CB reduced mass is obtained in the TE polarization and the lh-CB mass in the TM polarization. The deviations of the positions of dots and asterisks from a smooth line are caused by numerical errors.

The results of Fig. 9 can be interpreted in terms of the nonparabolic EMA description Eq. (13). The envelope coefficients $c_{n\mathbf{k}_\perp}^{F,\varepsilon}(k_\parallel)$ are determined by a finite integral over the $\varepsilon(\mathbf{k})$ dispersion of the band. In Fig. 10 a schematic picture of a nonparabolic dispersion is plotted (solid line). Considering

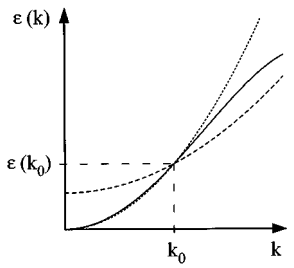

FIG. 10. Schematic picture of a nonparabolic band dispersion (solid line) and the parabolic approximations related to the energy effective mass (dotted line) and the curvature effective mass (dashed line).

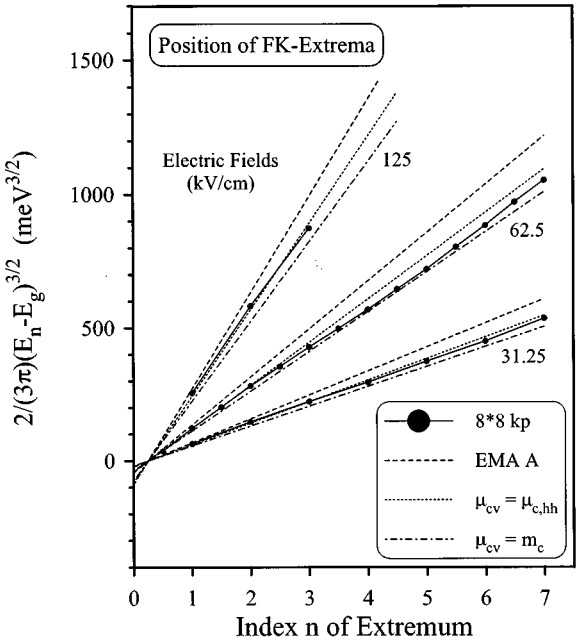

FIG. 11. Evaluation of electrical fields from the spectral positions of the FK oscillations as described in the text: a comparison of the results of various models.

a certain point k_0 on the dispersion line, the nonparabolic dispersion curve is only poorly represented if it is replaced with a purely parabolic curve that has the same *curvature* in k_0 (dashed line), corresponding to the curvature effective mass. It is, however, well approximated by a parabola that has the same origin and *intersects* the dispersion at the point k_0 (dotted line), corresponding to an energy effective mass. Hence the parabolic dispersion relations, corresponding to an energy effective mass, are a better approximation to the real, nonparabolic dispersion curves.

There is an important consequence of this result. The position of the minima of the FK oscillations can be described very precisely by an energy effective mass, which is only weakly dependent on the photon energy in wide-gap materials (small nonparabolicity). Therefore, an experimental determination of the electric field from the FK oscillations is fairly accurate in such materials if the Γ-point effective masses are well known and the energy dependence is neglected. A common procedure is to use Eq. (31) and the asymptotic expression for the zeros x_n of the Airy function

$$x_n = -\left[\frac{3\pi}{2}\left(n-\frac{1}{4}\right)\right]^{2/3}. \tag{37}$$

Substituting x_n leads to

$$\frac{2}{3\pi}(\hbar\omega_n - E_g)^{3/2} = (\hbar\,\theta_{cv})^{3/2}\left(n-\frac{1}{4}\right). \tag{38}$$

This equation is valid for integer values of n. It also holds for the maxima of the FK oscillations if n is equal to an integer plus 1/2. From a plot of the left-hand side of Eq. (38) versus n, using either experimental values for $\hbar\omega_n$ or, as done below, the values of our refined theories, one can deduce $(\hbar\,\theta_{cv})^{3/2}$ from the slope of the (ideally linear) curve.

$(\hbar\theta_{cv})^{3/2}$, on the other hand, is proportional to $F/\mu^{1/2}$. In order to show the validity of this method for the realistic band structure FK models, a comparison of the results of our simulations is shown in Fig. 11.

The values obtained within the 8×8 **k·p** model, which are considered to be a reference for the other models, are represented by dots and the solid lines. The EMA *A* (dashed lines) clearly yields too high slopes and, therefore, too high values of the field. The dotted lines are obtained if the reduced mass is assumed to be equal to the hh-CB mass within the 2D diagonal approximation or, equivalently, the EMA *B*. The dash-dotted lines are calculated for holes with an infinite effective mass. An unambiguous decision between the validity of these models is not possible, but the influence of the band coupling seems to imply a tendency towards the infinite-hole-mass model ($\mu_{cv}=m_c^*$) rather than the 2D diagonal approximation EMA *B* ($\mu_{cv}=\mu_{c,\mathrm{hh}}$). The latter is consistent with the observations in Fig. 8, where nearly equal oscillation periods are obtained for the 8×8 **k·p** model and the dispersionless holes.

As a consequence, the common method of field evaluation from the FK oscillation periods does not fail in large-gap semiconductors when band-structure effects are included because the deviations between the results of the simple EMA and realistic band-structure models are small. In principle, the energy dependence of the FK oscillations can also be used to determine the energy dependence of the energy reduced effective masses in the field direction. However, this method is applicable only in very pure material of a high crystalline quality since the observability of a large number of FK oscillations is necessary to obtain reliable results.

IV. CONCLUSION

We have calculated the field-dependent absorption spectra of GaAs (Franz-Keldysh absorption) in the framework of **k·p** theory. Our model is an extension of the well-known effective-mass theories of the FK effect accounting for the realistic band structure, including band nonparabolicity and band anisotropy. Two mechanisms influence the absorption characteristics: The field-induced intraband coupling of Bloch states along the field direction, which is also present in the EMA picture, and the coupling between states belonging to different bands. The former leads to the basic characteristics of FK absorption spectra, i.e., an absorption tail for photon energies below the band-gap energy and oscillations above, and the latter is responsible for the modifications introduced by the complicated band structure of real semiconductors. Three aspects of the problem have been discussed in particular: the implications on the density of states, which are also present in the zero-field limit, the polarization dependence of the spectra, and the width of the FK oscillations.

A direct comparison with effective-mass models shows that the CDOS is strongly increased for realistic band-structure models, especially for energies sufficiently above the band-gap energy. The increase of the CDOS, however, is not fully reproduced in the absorption spectra due to decreasing momentum matrix elements. The deviations from the EMA are relatively small for GaAs, but become more important for low-gap semiconductors such as InSb, as the amount of band coupling in increased.

For the field-dependent spectra we have demonstrated that a correct description of the polarization dependence is not possible in the EMA models since they either do not contain polarization-dependent momentum matrix elements at all (3D diagonal approximation) or become inconsistent in the zero-field limit (2D diagonal approximation). Nevertheless, the results of the calculations within the full **k·p** model have shown that the basic FK absorption characteristics can be well understood if one assumes that the hh and the lh bands are decoupled. The absorption is dominated by the hh-CB transitions if the polarization is perpendicular to the static field (TE), whereas for the case of parallel polarization (TM) the lh-CB transitions prevail. In this respect the system behaves like a quasi-2D system. This property can be shown exactly in the limiting case of energies deep in the band gap, but it is astonishing for energies above the band gap, where a stronger influence of state mixing would be expected. As a consequence, the 2D diagonal approximation yields good results, although it is not able to account for the amount of the difference between TE and TM polarization in the absorption tails. A comparison with experimental results confirmed the theoretical findings.

The nonparabolicity of the band dispersions is reflected in the period lengths of the FK oscillations. We have shown that they depend almost exclusively on the zero-field band dispersions, whereas the explicit band-to-band coupling terms mainly affect the overall magnitude of the absorption. An evaluation of the oscillation maxima shows that their position can be described in terms of an energy-dependent effective mass, obtained from the realistic combined electron-hole band dispersions, evaluated at an energy value corresponding to the photon energy. Basically this effect should be taken into account if one tries to evaluate the electric field from the position of the FK oscillation extrema. In large-gap semiconductors such as GaAs, however, it is comparably small and can be neglected for a first approximation. Nevertheless, even in GaAs the deviations are such that the series of oscillation extrema in TE polarization are better described assuming an infinite hole mass rather than realistic Γ-point values for the hh mass.

In summary, the **k·p** method has proved to be a very powerful tool to describe these effects. However, the numerical efforts are enormous and inhibit a further *a priori* inclusion of the Coulomb interaction. In spite of this deficiency our spectra provide good agreement with available experimental findings. More detailed experimental investigations, possibly in lower-gap materials, should be able to reveal further details of our theoretical predictions.

APPENDIX A: THE k·p HAMILTONIAN

The lattice-periodic functions $u_{n\mathbf{0}}$ are unambiguous except for a free overall phase for the Clebsh-Gordon coefficients if they are chosen to have both the symmetry of angular-momentum eigenstates and the symmetry of the double group at the Γ-point of the crystal. We choose for the phases the Condon-Shortley convention

$$\langle jj(j_1,j_2)|[|j_1j_1\rangle\otimes|j_2j_2\rangle]=1, \tag{A1}$$

where $j=j_1+j_2$ and j_1 and j_2 are the quantum numbers of respectively, the absolute value of angular momentum of the

spin and the orbital angular momentum of an electron in an atom-like state u. The resulting states are shown in Table I, the 8×8 $\mathbf{k}\cdot\mathbf{p}$ Hamiltonian expanded in these states is given in Table II.

APPENDIX B: ORTHONORMALITY OF THE FK EIGENSTATES

To prove the orthonormality of the FK eigenstates obtained by Eq. (7) we proceed in two steps. First we show that the states for different initial conditions $\mathbf{k}_\perp$ are orthogonal; second we demonstrate that the states for the same $\mathbf{k}_\perp$ are orthonormal. With the form of the solutions (6) the inner product between two states of different $\mathbf{k}_\perp$ is

$$\begin{aligned}\langle \Psi_{\mathbf{k}_\perp'} \Psi_{\mathbf{k}_\perp}\rangle &= \frac{\Omega^{2/3}}{4\pi^2}\sum_{n,n'}\int dk_\parallel \int dk_\parallel' \int d\mathbf{x} e^{i(\mathbf{k}-\mathbf{k}')\cdot\mathbf{x}} u_{n\mathbf{0}}(\mathbf{x}) \\ &\quad\times u^\star_{n'\mathbf{0}}(\mathbf{x}) c_{n\mathbf{k}_\perp}(k_\parallel) c^\star_{n'\mathbf{k}_\perp'}(k_\parallel') \\ &= \frac{\Omega^{2/3}}{4\pi^2}\delta(\mathbf{k}_\perp-\mathbf{k}_\perp') \\ &\quad\times\sum_n \int dk_\parallel u_{n\mathbf{0}}(\mathbf{x}) u^\star_{n\mathbf{0}}(\mathbf{x}) c_{n\mathbf{k}_\perp}(k_\parallel) c^\star_{n\mathbf{k}_\perp}(k_\parallel),\end{aligned} \tag{B1}$$

where we have used that $\langle \chi_{n\mathbf{k}} | \chi_{n'\mathbf{k}'}\rangle = \delta_{nn'}\delta(\mathbf{k}-\mathbf{k}')$ [with χ as defined in Eq. (3); cf. Ref. 21].

To prove that the states for different initial conditions $\mathbf{c}^{(i)}$ are orthonormal it is sufficient to show that $\langle \mathbf{c}^{(i)}, \mathbf{c}^{(i')}\rangle = \delta_{ii'}$, where the inner product is defined by $\langle \mathbf{a},\mathbf{b}\rangle = \Sigma_m \int_{\Delta_\parallel} dk_\parallel a_m^\star(k_\parallel) b_m(k_\parallel)$. The states belonging to the initial conditions (8) clearly fulfill this orthonormality if there is a unitary operator $U(k_\parallel)$ with

$$\mathbf{c}^{(n)}(k_\parallel) = U(k_\parallel)\mathbf{c}^{(n)}(0). \tag{B2}$$

This unitary operator can be constructed in analogy to the time-evolution operator in time dependent perturbation theory:

$$U(k_\parallel) = \tau \exp\left\{ \frac{i}{eF}\int_0^{k_\parallel} dk_\parallel' (H^{(\mathbf{k}_\perp, k_\parallel')\cdot\mathbf{p}} - \varepsilon)\right\}. \tag{B3}$$

Since, in general, the operators $H^{\mathbf{k}\cdot\mathbf{p}}$ for different $\mathbf{k}$ do not commute, the operator τ has to be introduced, which arranges them after increasing $k_\parallel$ in the series expansion of the exponential function. U is completely analogous to the time-evolution operator if one identifies $k_\parallel$ with t, $(1/eF)[H^{\mathbf{k}\cdot\mathbf{p}} - \varepsilon]$ with $(-1/\hbar)H(t)$, and τ with Dyson's time-ordering symbol. Thus $U(k_\parallel)$ as defined by Eq. (B3) is the operator wanted.

*Present address: Fachbereich Physik und Zentrum für Materialwissenschaften, Philipps Universität Marburg, Renthof 5, D-35032 Marburg, Germany.

[1] W. Franz, Z. Naturforsch. **13**, 484 (1958).
[2] L.V. Keldysh, Zh. Éksp. Teor. Fiz. **34**, 1138 (1958) [Sov. Phys. JETP **34**, 788 (1958)].
[3] D.E. Aspnes, Phys. Rev. **147**, 554 (1966).
[4] D.E. Aspnes, Phys. Rev. **153**, 972 (1967).
[5] K. Tharmalingam, Phys. Rev. **130**, A2204 (1963).
[6] C.M. Penchina, Phys. Rev. **138**, A924 (1965).
[7] J.D. Dow and D. Redfield, Phys. Rev. B **1**, 3358 (1970).
[8] D.F. Blossey, Phys. Rev. B **2**, 3976 (1970).
[9] H.D. Rees, J. Phys. Chem. Solids **29**, 143 (1968).
[10] I. Galbraith and B. Ryvkin, J. Appl. Phys. **74**, 4145 (1993).
[11] N. Linder, W. El-Banna, U.D. Keil, K. Schmidt, G.H. Döhler, J.N. Miller, and K.J. Ebeling, SPIE Proc. **1286**, 359 (1990).
[12] L.V. Keldysh, O.V. Konstantinov, and V.I. Perel, Fiz. Tekh. Poluprovodn. **3**, 1042 (1969) [Sov. Phys. Semicond. **3**, 876 (1970)].
[13] E.O. Kane, in *Semiconductors and Semimetals*, edited by R.K. Willardson and A.C. Beer (Academic, New York, 1966), Vol. 1, p. 75.
[14] H. Sheen and F. H. Pollak, Phys. Rev. B **42**, 7097 (1990).
[15] M. Cardona, N.E. Christensen, and G. Fasol, Phys. Rev. B **38**, 1806 (1988).
[16] P. Löwdin, J. Chem. Phys. **19**, 1396 (1951).
[17] H. Haug and S.W. Koch, *Quantum Theory of the Optical and Electronic Properties of Semiconductors* (World Scientific, Singapore, 1993).
[18] *Numerical Data and Functional Relationships in Science and Technology*, edited by O. Madelung, M. Schulz, and H. Weiss, Landolt-Börnstein, New Series, Group III, Vol. 17, Pt. a (Springer, Berlin, 1982).
[19] H. Jones, *The Theory of Brillouin Zones and Electronic States in Crystals* (North-Holland, Amsterdam, 1975).
[20] The absorption in TE polarization depends on the relative angle ϕ between $\hat{\mathbf{e}}$ and $\hat{\mathbf{k}}_\parallel$. For $\mathbf{F}\parallel[001]$ one thus needs all states for $0\leqslant\phi<\pi/2$. Nevertheless, it is sufficient (in the diamond lattice) to calculate the states for $0\leqslant\phi<\pi/4$; the others can be derived from those by application of the crystal symmetry $(x,y,z)\rightarrow(y,x,z)$.
[21] J.M. Luttinger and W. Kohn, Phys. Rev. **97**, 869 (1955).
[22] M. Altarelli, in *Heterojunctions and Semiconductor Superlattices*, edited by G. Allen *et al.* (Springer, New York, 1986).
[23] M. Yamanishi and I. Suemune, Jpn. J. Appl. Phys. **23**, L35 (1984).
[24] A. Baldereschi and N.O. Lipari, Phys. Rev. B **3**, 439 (1971).
[25] A. Baldereschi and N.O. Lipari, Phys. Rev. B **8**, 2697 (1973).
[26] F.K. Reinhart, Appl. Phys. Lett. **22**, 372 (1973).
[27] N.K. Dutta and N.A. Olsson, Electron. Lett. **20**, 634 (1984).
[28] B. Knüpfer, P. Kiesel, M. Kneissl, S. Dankowski, N. Linder, G. Weimann, and G.H. Döhler, IEEE Photon. Technol. Lett. **5**, 1386 (1993).
[29] M. Ruff, D. Streb, S.U. Dankowski, S. Tautz, P. Kiesel, B. Knüpfer, M. Kneissl, N. Linder, and G.H. Döhler, Appl. Phys. Lett. **68**, 2968 (1996).
[30] C. Van Hoof, K. Deneffe, J. De Boeck, D.J. Arent, and G. Borghs, Appl. Phys. Lett. **54**, 608 (1989).
[31] M. Sydor, J.R. Engholm, M.O. Manasreh, C.E. Stutz, L. Liou, and K.R. Evans, Appl. Phys. Lett. **56**, 1769 (1990).
[32] H.D. Rees, Solid State Commun. **5**, 365 (1967).
[33] G. Dresselhaus, Phys. Rev. **100**, 580 (1955).
[34] J.S. Blakemore, *Key Paper in Physics, No. 1, Gallium Arsenide* (AIP, New York, 1987).